



Mechanical Properties and Failure Characteristics of Hybrid Bonded-Bolted GFRP/Al Joints under Dynamic Tensile load

Hao Li¹ · Wei Du¹ · Xianming Meng² · Sai Zhang² · Yuxuan Cui¹ · Wenchao Guo¹ · Shipeng Li¹

Received: 5 October 2023 / Accepted: 5 December 2023 / Published online: 5 January 2024
© The Author(s), under exclusive licence to Springer Nature B.V. 2024

Abstract

In this study, the mechanical properties and failure characteristics of bolted and hybrid bonded-bolted GFRP/Al joints under different loading speeds were investigated. The failure process and strain evolution were recorded using high-speed cameras and digital image correlation (DIC) techniques. The micro-morphology of the fracture was also investigated to explore the effect of loading speed on the fracture mode. The results showed that the peak load, failure displacement, and energy absorption for all joints were sensitive to the loading speed. The peak load and energy absorption of the hybrid joints were higher than that of the bolted joints under both static and dynamic loading. The loading speed had no significant effect on the failure mode of GFRP material in bolted joints, which were all shear-out failures. While for the hybrid joint, the addition of the adhesive layer changed the failure mode of GFRP material from shear-out failures to tension failures. As the loading speed increased, the final failure area of GFRP in hybrid joints gradually decreased. In hybrid joints, a greater amount of bearing damage preceded a final tension failure in GFRP material with the increase in loading speed. The fracture surface became flatter and the pulled-out fiber bundles were more integral due to the fact that cracks within the material could not extend sufficiently at high loading rates.

Keywords GFRP laminate · Hybrid joint · High-speed tensile · Failure behavior and mechanism

1 Introduction

Fiber-reinforced plastics (FRPs) have extensive applications in diverse fields including aerospace, automotive industry, marine vessels, and constructions, owing to their distinctive attributes of specific strength, specific stiffness, and lightweight characteristics [1, 2].

✉ Hao Li
haolitju@tju.edu.cn

¹ Key Laboratory of Mechanism Theory and Equipment Design of Ministry of Education, Tianjin University, Tianjin, China

² China Automotive Technology and Research Center Co., Ltd, 68 East Xianfeng Road, Tianjin, China

Typical fiber-reinforced plastics are carbon fiber reinforced plastics (CFRP) and glass fiber reinforced plastics (GFRP). CFRP stands out for its superior strength and stiffness levels. CFRP is preferred for high-end products that require high strength and lightweight due to its high cost [3, 4]. Compared to CFRP, GFRP possesses notable advantages such as excellent dielectric properties, non-flammability, and cost-effectiveness, playing an irreplaceable role in certain domains [5, 6]. With the widespread use of composites, the joining of composite materials with other materials becomes a critical issue.

Commonly employed joining methods are mechanical joining (such as riveting and bolting), adhesive bonding, and welding [7–10]. Mechanical joints are efficient and capable of bearing substantial loads, but the bolt hole destroys the continuous fiber, resulting in a stress concentration at the hole edge. Bonded joints are effective but have limitations in carrying heavy loads. Hybrid bonded-bolted/riveted joints, which integrate mechanical joining and adhesive bonding, have been demonstrated to combine the advantages of both methods, thereby enhancing joint performance. For example, Chen et al. [11] investigated the quasi-static tensile properties of CFRP/Al bonded, riveted, and hybrid joints. The results showed that hybrid joints obtained higher peak loads and higher energy absorption levels compared to riveted and bonded joints; the addition of adhesive to riveted joints can prevent the formation of catastrophic damage. Paliwal et al. [12] investigated the failure mechanisms of CFRP bolted, bonded, and hybrid joints under quasi-static loading and concluded that hybrid joints had stronger damage tolerance. In typical circumstances, joints endure consistent quasi-static or cyclic loads. However, the mechanical behavior of materials under dynamic loading differs from that under static loading, and it is essential to investigate the behavior of joints under dynamic loads.

Several scholars have conducted investigations on the performance of composite material joints under dynamic loading conditions. It was demonstrated that varying joint structures exhibit diverse behaviors in response to distinct loading rates. Jiang et al. [13] investigated the behavior of CFRP/Al electromagnetic self-piercing riveted joints under high-speed loading, and the results showed that the joints had high shear resistance at higher loading speeds; the energy absorption of the joints decreased with the increase of loading speed, and the loading speed had a significant effect on the damage mode. Zuo et al. [14] investigated the performance of CFRP/Ti pinned single lap joints under high-speed loading, and the results showed that the ultimate load decreased with the increase of loading speed; the failure mode was dominated by CFRP damage, which started to fail in the bearing damage mode, but eventually failed in the tearing damage mode. Egan et al. [15] investigated the performance of CFRP bolted joints under high-speed loading and they also found that the shear performance of the joint decreased with increasing loading rate. Heimbs et al. [16] investigated the performance of CFRP bolted joints under static loading, 2 m/s, and 10 m/s loading rates. It was concluded that there was no obvious rate sensitivity in terms of damage modes and force-displacement behavior of single-bolted joints. Whereas, the damage modes and force-displacement behavior of double bolted joints were rate sensitive.

Besides mechanical joints, the investigation of the performance of bonded joints under different loading rates was also published. Liu et al. [17] investigated the performance of CFRP/Al bonded joints at 1.3 mm/min, 0.1 m/s, 1 m/s, and 5 m/s tensile rates. It can be obtained that the strength of the joints increased with the increase of the loading rate, and the damage mode of the joints gradually changed from the bond damage mode to the fiber tear damage mode. Wang et al. [18] investigated the performance of CFRP/Al bonded joints at 2 mm/min, 4 m/s, 8 m/s, and 12 m/s tensile rates and the shear strength of the bonded joints was found to increase with the increase of loading rate.

However, the research on the performance of joints under dynamic loading mainly focuses on CFRP, and the dynamic tensile properties of GFRP joints have not yet been studied. Additionally, the current research only focuses on the dynamic loading mechanical properties and failure mechanism of a single mechanical joint or bonded joint, while mechanical properties and failure mechanisms of hybrid bonded/bolted joints under dynamic loading are not clear. Therefore, hybrid bonded-bolted joints and bolted joints were selected to study the effects of different loading speeds (2 mm/min, 1 m/s, 5 m/s, and 10 m/s) and adhesive layers on the mechanical properties and failure mechanism of joints in this paper. The corresponding mechanical properties were analyzed and compared in detail. The failure process of the joints was recorded using high-speed cameras, and the full-field strain of the failure process was analyzed by the digital image correlation (DIC) method. The microscopic fracture was characterized using a scanning electron microscope (SEM). The failure modes and mechanisms of the joints under different loading speeds were discussed and analyzed.

2 Experimental Work

2.1 Materials and Specimen Preparation

In this study, the substrates of joints were GFRP laminates and 6061 aluminum alloy sheets. GFRP laminates (Weihai Guangwei Composites Co., Ltd) were fabricated by the technique of prepreg vacuum bagging, composing of unidirectional fiber fabrics and epoxy resin. The total thickness of GFRP laminates (made of 20 layers of unidirectional fiber prepreg with the stacking sequence of [0/90/45/-45]s) was 3 mm. The M6 Q235 steel bolts were implemented to fabricate joints of GFRP and aluminum sheets. The two-component epoxy structural adhesive Araldite 2015 (Huntsman, USA) was utilized to bond the GFRP laminate and aluminum alloy sheets. Their mechanical properties are presented in Table 1.

Figure 1 shows the detailed geometric parameters of the hybrid joint. The GFRP laminates and aluminum alloy substrates were cut to the dimensions of 100 mm × 25 mm using a 4-axis CNC machining center. Before the bonding operation, the substrate's overlap area was unidirectionally grinded (at a direction of 45° angle along the material's length) using 300-grit sandpaper. Subsequently, the substrate was cleansed with acetone to remove contaminants on the surface (e.g. oxidized layers, dust, and grease). The thickness (0.5 mm) of the adhesive layer was controlled using a specifically designed mold. The adhesive specimens were heated at 60 °C for 5 h using a constant temperature oven to reach a certain

Table 1 Mechanical properties of GFRP, 6061 aluminum alloy, Q235 steel bolt, and Araldite 2015 adhesive [19–21]

Characteristic	GFRP unidirectional	6061 aluminum alloy	Q235 steel bolt	Araldite 2015 adhesive
Density(g/cm ³)	1.8	2.7	7.8	1.54
Young's modulus (GPa)	42	68.9	202	1.85
Poisson's ratio	0.34	0.33	0.3	0.33
Tensile strength (MPa)	950	310	445	21.6

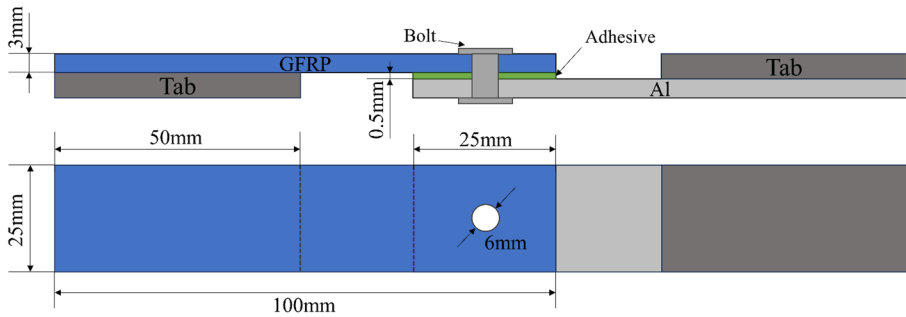


Fig. 1 Geometric parameters of hybrid joint

strength and then cured naturally at room temperature for 5 days to achieve their best mechanical properties. Before conducting the bolting operation on the cured GFRP/Al specimens, the joining holes were drilled at the center of the overlap area. A preload torque of 3.5 N was applied to the bolts. Substrate dimensions, hole sizes, and preload force levels in bolted joints were the same as those in hybrid joints. To reduce the effects of eccentric loading in tensile tests, tabs of the same size were pasted at both ends of the single-lap joints as a clamping member.

2.2 Experimental Procedure

Static tensile tests and dynamic tensile tests were conducted on both bolted joints (BJ) and hybrid joints (HJ). The static load test was conducted using a universal testing machine with a tensile speed of 2 mm/min. The dynamic load test was carried out on a high-speed tensile testing machine (Zwick HTM16020), which can provide a maximum tensile force of 100kN and tensile speed of 0.01 m/s–100 m/s. The high-speed tensile test equipment is shown in Fig. 2. The dynamic tensile speeds were set to 1 m/s, 5 m/s, and 10 m/s, respectively. High-speed cameras were utilized to photograph the front, back, and side of the

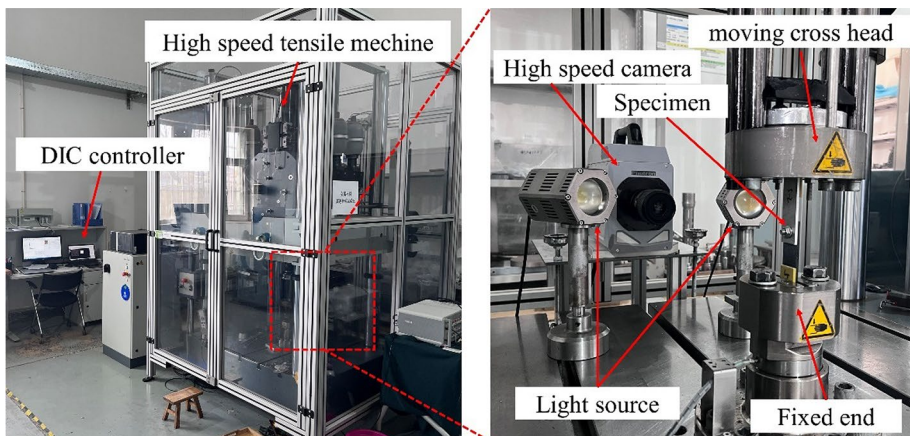


Fig. 2 High-speed tensile test equipment

joint to record the failure process in detail. The frame rates of the high-speed camera were selected based on the loading speeds. Frame rates of 20,000, 50,000, and 100,000 frames per second (fps) were set for loading speeds of 1 m/s, 5 m/s, and 10 m/s, respectively. The lap area was sprayed with black and white paint to create a scatter for strain field analysis. In order to analyze the strain variation of the substrate during the tensile process, longitudinal plane engineering strains were calculated using XTDIC-2D software. The microscopic failure mechanisms of adhesive joints were analyzed via an SEM.

3 Result and Discussion

3.1 Dynamic Mechanical Responses

Figure 3 depicts the load-displacement (L-D) curves of bolted and hybrid joints under different loading speeds. Comparing Fig. 3(a) and (b), it could be seen that the L-D curves of bolted joints under quasi-static load were smoother than those under dynamic load. The fluctuant phenomenon was the typical responses (multilayer progressive damage) of the composite at dynamic load [22]. From Fig. 3(c), it can be seen that the L-D curves can be divided into the adhesive load-carrying stage (stage I) and the bolt load-carrying stage (stage II). The L-D curves of hybrid joints exhibited significant oscillations during stage II, which was caused by the impulse when the dynamic load excited the test system [23]. The

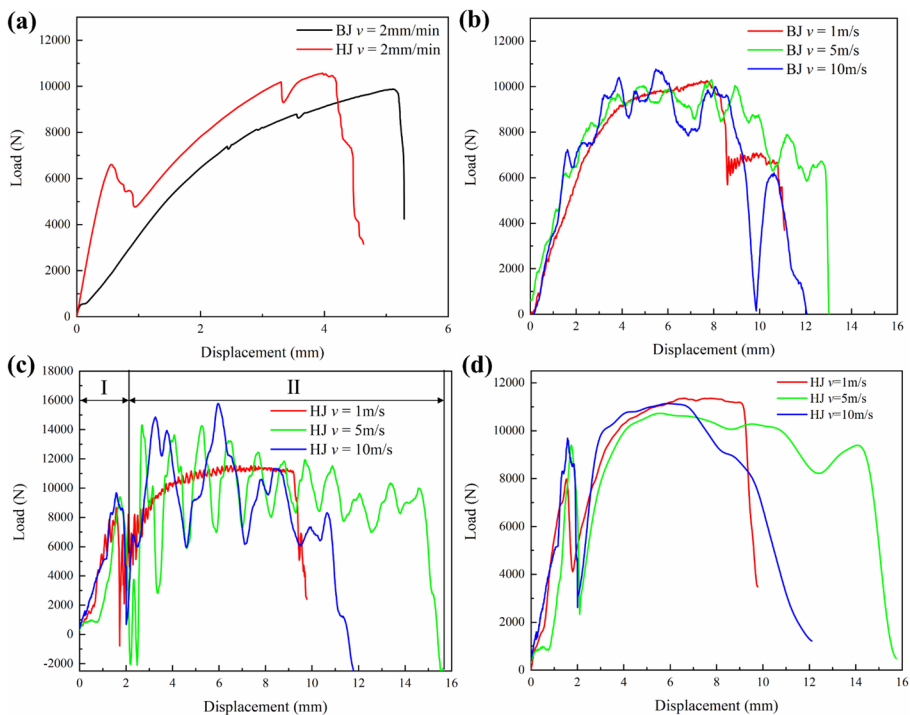


Fig. 3 L-D curves of **a** bolted and hybrid joints under static load, **b** bolted joints under dynamic load, **c** raw and **d** filtered L-D curves of hybrid joints under dynamic load

impulse signals were mainly from the damage of adhesive, which means that the cases with more damage had more evident oscillation of mechanical responses. The filtering method can be used to mitigate this issue [24]. To be specific, the upper and lower envelope of the oscillation curve were calculated, and their average value was the final filtered mechanical response for further analyses [25]. The filtered curves are shown in Fig. 3(d). The filtered curves can be used to analyze the mechanical properties of hybrid joints under dynamic load, as shown in Fig. 4.

Figure 4(a) shows the peak loads of bolted and hybrid joints at different loading speeds. It can be obtained that the peak load of the bolted joints increased with the increase in loading speed. This is due to the rate sensitivity of GFRP material. The peak load of hybrid joints of 1 m/s loading speed was higher than that of 2 mm/min, while the peak load of 5 m/s and 10 m/s was lower than that of 1 m/s. The difference in peak loads at different loading speeds may be due to the failure mode was different at different loading speeds. The peak load of the hybrid joints was higher than that of bolted joints at the same loading speed, indicating that the hybrid joints had better load-carrying capacity under both static and dynamic loading.

The failure displacement and energy absorption of bolted and hybrid joints at different loading speeds are presented in Fig. 4 (b) and (c). The failure displacement and energy absorption of both bolted and hybrid joints exhibited similar trends with changes in loading speed. Specifically, the failure displacement and energy absorption increased with the increase of loading speed when the loading speed was below 5 m/s but decreased significantly when the loading speed reached 10 m/s. Normally, the failure displacement and energy absorption of the joints were significantly decided by the deformation of the matrix material [26, 27]. The joint structure used in this experiment consisted of three materials: GFRP, aluminum alloy, and adhesive. GFRP and adhesive had little plastic deformation during the loading process due to their brittle material characteristics. However, more obvious plastic deformation occurred on the aluminum alloy during the loading process, and the amount of deformation varied with the change in loading speed, which in turn led to different failure displacements and energy absorption. The specific reasons for this will be elaborated in the next section. Under the same loading speed, the energy absorption of the hybrid joints was higher than that of the bolted joints. The peak load of the hybrid joints increased by 8.38%, 11.28%, 3.63% and 2.64% compared to that of the bolted joints at loading speeds of 2 mm/min, 1 m/s, 5 m/s and 10 m/s, respectively. The energy absorption of the hybrid joints increased by 6.46%, 9.56%, 30.97% and 23.45% compared to the bolted joints at loading speeds of 2 mm/min, 1 m/s, 5 m/s and 10 m/s, respectively. These

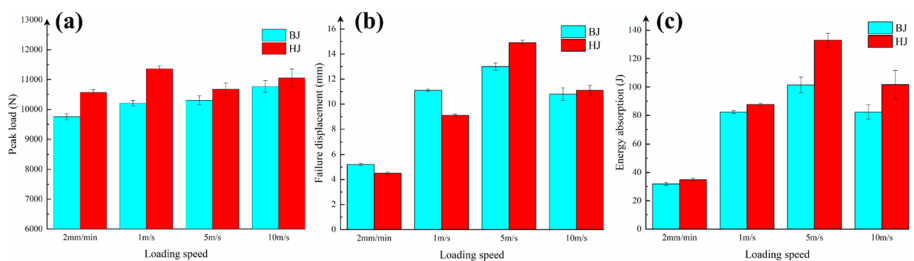


Fig. 4 Mechanical properties of bolted and hybrid joints: **a** peak load, **b** failure displacement, **c** energy absorption

indicated that the hybrid joints had a better energy absorption capacity under both static and dynamic loading conditions.

3.2 Failure Mechanism Analysis

The failure modes of GFRP in bolted joints under different loading speeds are shown in Fig. 5. Extrusion deformation was observed around the composite hole. Two distinct cracks expanded in the transverse and longitudinal directions, resulting in the separation of the laminates. It can be concluded that the failure mode of GFRP under static loading was a mixed failure mode of bearing failure and cleavage failure. For the dynamic loading condition, the joint failure modes did not show a significant correlation with the loading speed. Taking the failure mode at 10 m/s loading speed as an example, the final failure mode of the joints was a shear-out failure for all GFRP laminates.

The failure modes of the GFRP and the adhesive layer in the hybrid joints are shown in Fig. 6. The failure mode of GFRP in hybrid joints was mainly a tension failure, which was quite different with that in bolted joints. This may be due to the fact that the hole stress state of the GFRP in the hybrid joint was changed by the viscous action of the adhesive. The yield strength of the hole was increased, ultimately leading to a different failure mode. The failure mode of the hybrid joint under 1 m/s and 5 m/s loading speed was similar to that under static loading, with the load-carrying part being pulled out. At a loading speed of 10 m/s, the GFRP failure mode changed to shear-out failure. The area of the fractured part (Region I) decreased with the increase of the loading speed. Compared to static loading, the failure area of GFRP was reduced by 11.09%, 45.35% and 90.75% at 1 m/s, 5 m/s and 10 m/s loading speeds, respectively. As can be seen from the side view, the thickness (h_L and h_R) and length of the tensile fractured part also decreased with the increase of the loading speed. The reason for this phenomenon is related to the failure behavior of composite materials at high strain rates. During the manufacturing process of composites, many initial defects such as tiny cracks and porosity were inevitably generated within the material [28–30]. When subjected to loads, cracks would expand along the location of internal defects, eventually leading to

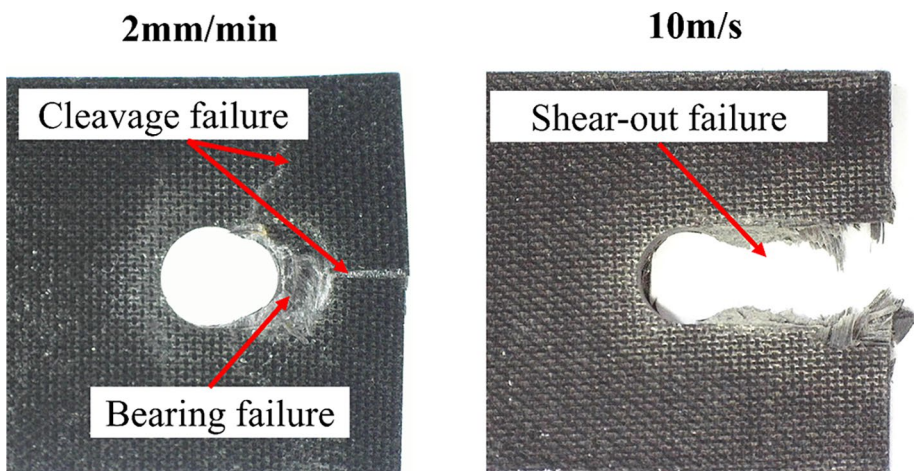


Fig. 5 Failure modes of GFRP in bolted joints under different loading speeds

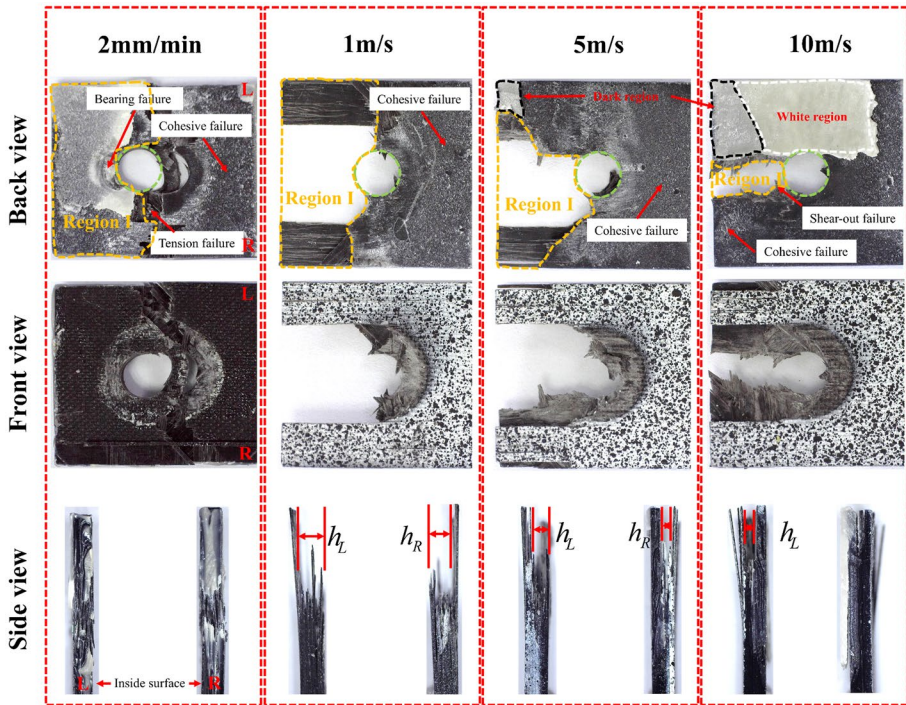


Fig. 6 Failure modes of GFRP and adhesive layer in hybrid joints under different loading speeds

material damage. When the loading speed was relatively low, cracks had sufficient time to propagate, resulting in a larger failure area. However, as the loading speed increased, the entire loading process became shorter, and cracks did not have enough time to propagate, consequently leading to a gradual reduction in the failure area of GFRP.

From the experimental results, the residual adhesive can be found on both CFRP and aluminum alloy interfaces. The failure mode of the adhesive layer was cohesive damage at all loading speeds. The difference was that the failure surface became smoother and exhibited the characteristics of brittle fracture as the loading speed increased. Under static loading, the adhesive layer showed an obvious “whitening” phenomenon, which was due to the excessive deformation of the adhesive. From the residual adhesive, one can see that the adhesive was partly dark and partly white at 5 m/s and 10 m/s loading speed. The dark portion indicated that the adhesive layer had been subjected to high peel stresses and less shear stresses. It indicated that the adhesive layer was subjected to a small shear deformation under high-speed loading. This was related to the behavior of the adhesive layer under high strain rate. The adhesive material used here (Araldite 2015) is an epoxy polymer. Under quasi-static tension, its entangled molecular chains had time to reorient themselves to align with the loading direction. As a result, the adhesive was capable of plastic deformation and failure in the form of ductile fracture. In contrast, at high loading speeds, the molecular chains did not have enough time to rearrange themselves, resulting in less plastic deformation and brittle fracture.

The failure mode of aluminum alloy is shown in Fig. 7(a). The aluminum alloy joint hole was elongated and the aluminum alloy deformed along the perpendicular to the

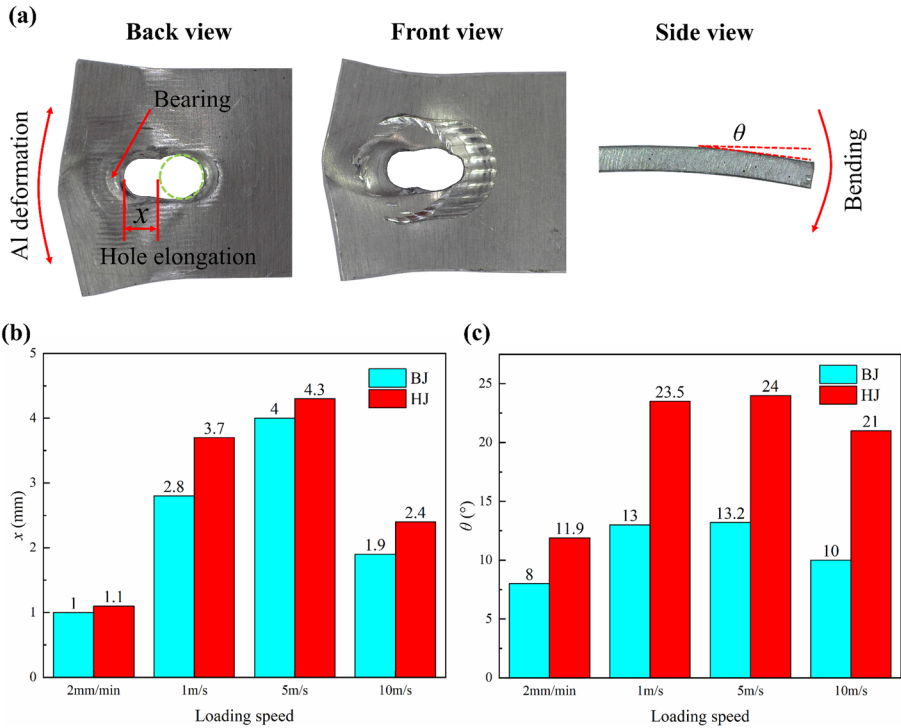


Fig. 7 Failure modes of aluminum alloy under different loading speed: **a** failure mode, **b** deformation elongation x of the hole, **c** bending angle θ

shear direction. The side view showed that the aluminum alloy was bent. The deformation elongation x of the hole and the bending angle θ of the aluminum alloy changed under different loading speeds, as shown in Fig. 7(b) and (c). The elongation of the holes and the bending angle of the aluminum alloy under dynamic loading were much larger than those under static loading. In the range of loading speed less than 5 m/s, the aluminum alloy hole deformation and bending angle increased with the increase of loading speed but decreased at 10 m/s loading speed. This was related to the strain rate effect of aluminum alloys. According to the related research [28–30], the strength, hardness, and plasticity of aluminum alloys vary with the strain rate. Generally, the plasticity of aluminum alloys increases with the strain rate and the hardening rate increases with the strain rate. At a loading speed of 10 m/s, the hardening rate of the aluminum alloy might be greater than the change in plasticity with strain rate, resulting in a decrease in the deformation of the aluminum alloy. These changes explained the decrease in joint energy absorption at 10 m/s loading speed.

The failure process of hybrid joints can be divided into the adhesive load-bearing stage, the aluminum alloy deformation stage, and the GFRP failure stage, as shown in Fig. 8(a). In the first stage, the joint was bent under the action of load and the adhesive layer. After the failure of the adhesive layer, the joint wobbled because of the energy released by the failure of the adhesive layer. Subsequently, it entered the bolt load-bearing stage. It can be seen that the aluminum alloy had obvious displacement, while the

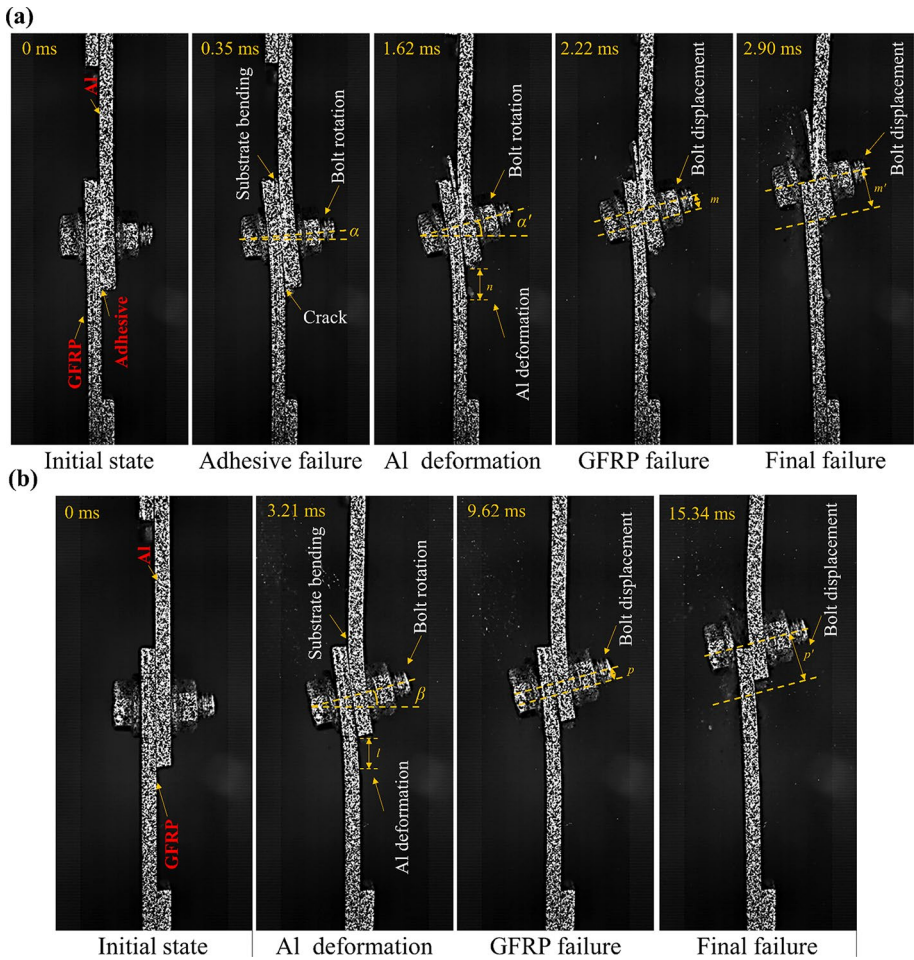


Fig. 8 Failure process (side view) of: **a** hybrid joint at 10 m/s loading speed, **b** bolt joint at 1 m/s loading speed

bolt did not move. It was inferred that during this period there was no obvious damage in the GFRP material. In the third stage, when the external load reached the yield limit of the GFRP material, the GFRP failed, leading to the displacement of the bolt. The failure process of the bolted joint had only the aluminum alloy deformation stage and the GFRP failure stage as there was no adhesive layer in action, as shown in Fig. 8(b).

The frontal view of the joint failure process under different loading speeds is shown in Fig. 9. The failure process of bolted joints under different loading speeds was similar, and the failure process of bolted joints was illustrated by the failure process under 10 m/s loading speed, as shown in Fig. 9(a). As can be seen from the figure, GFRP eventually cleaved after bearing failure. The failure process of hybrid joints under different loading speeds is shown in Fig. 9(b). The tension failure of the GFRP occurred directly after the deformation stage of the aluminum alloy at 1 m/s loading speed. At 5 m/s and 10 m/s loading speeds, bearing failure occurred first, followed by tension failure.

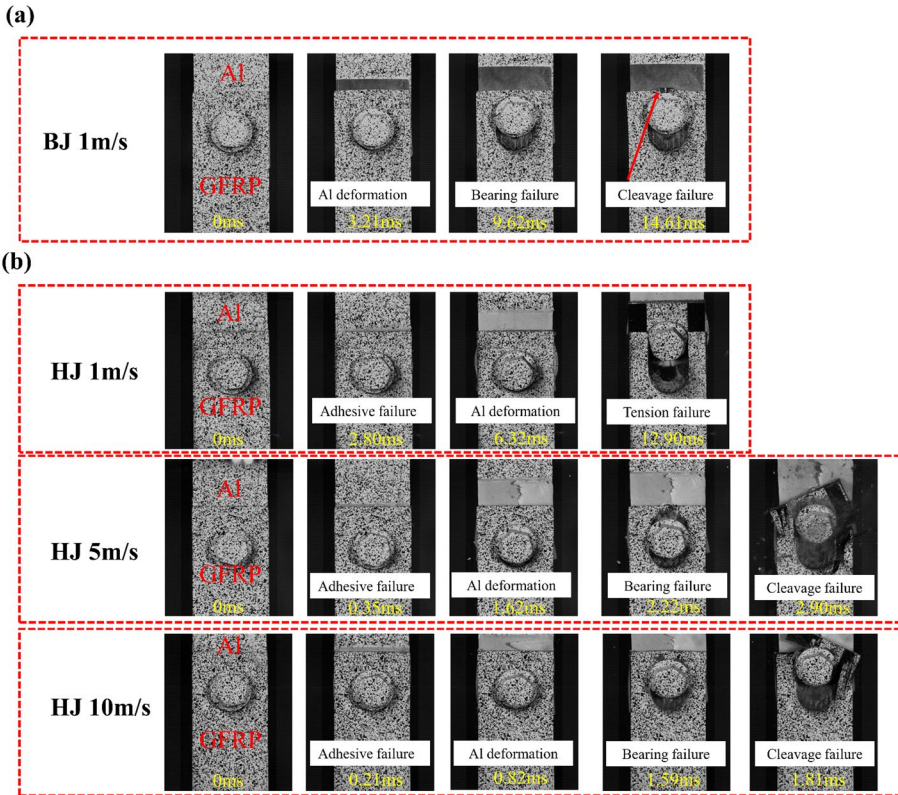


Fig. 9 Failure process of joints at different loading speeds(front view): **a** bolted joints, **b** hybrid joints

The addition of the adhesive layer significantly changed the failure mode of the joints, and the failure of the GFRP changed from shear-out failure to tension failure. This is due to that the yield strength of the joint hole can be enhanced due to the viscous effect of the adhesive. The loading speed has no significant effect on the failure mechanism of single bolted joints, but has a significant effect on the hybrid joints. As the loading speed increased, the final failure area of GFRP in hybrid joints gradually decreased. GFRP failed abruptly from a net-tension failure with almost no prior bearing damage at lower loading speeds (2 mm/min and 1 m/s). With the increase in loading speed, more amount of bearing damage preceded a final tension failure. This was due to the fact that as the loading speed increased, the loading time became very short. Consequently, the concentrated stress around the GFRP hole did not have sufficient time to dissipate, causing the damage to GFRP to be increasingly concentrated around the holes.

To further analyze the reasons for the changes in the failure process of the hybrid joints, full-field strain analysis was conducted on the GFRP and Al plates during the tensile process. The strain-time curves of four measuring points on the surface of each plate were plotted based on the DIC measurement data. The selected locations of the measuring points and the strain-time curves are shown in Fig. 10. It can be seen that due to the symmetry of the joint, the strain-time curves of points 3 and 4 are almost the same and remain constant during the entire loading process. The strain values of points 1 and 2, which were

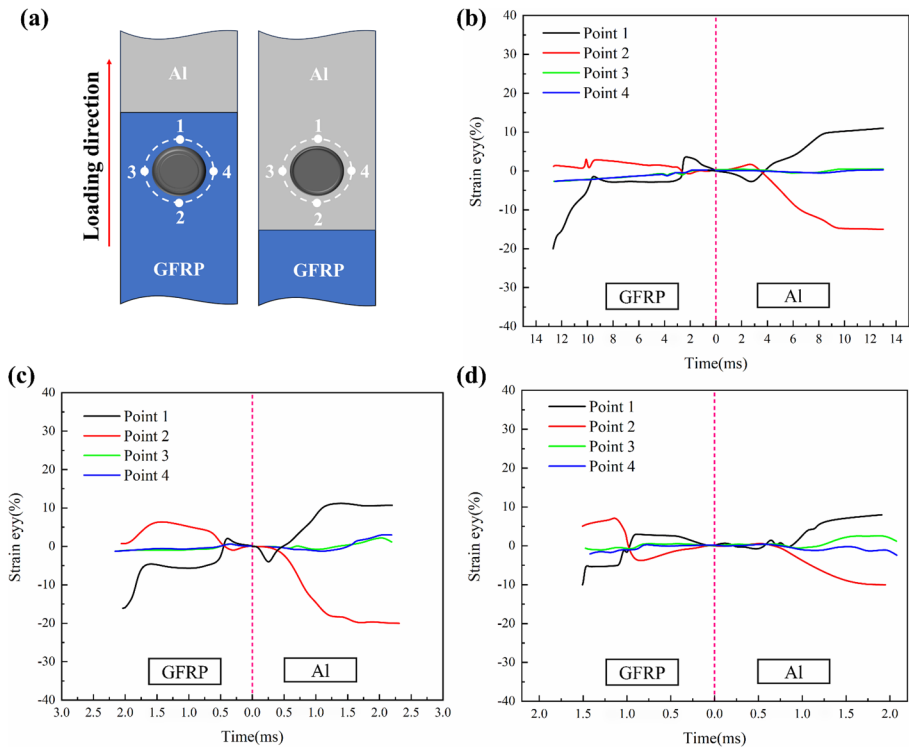


Fig. 10 a The schematic diagram of measuring points for the specimen; variation of strain at measured points of hybrid joints under different loading speeds: **b** 1 m/s, **c** 5 m/s, **d** 10 m/s

the locations of the largest substrate deformation, varied greatly with time. The maximum strain value of point 1 of the GFRP before failure decreased as the loading speed increased. This was due to the reason that GFRP became more brittle with the increasing strain rate, which resulted in GFRP failing with smaller strains at higher loading speeds. The aluminum alloy was subjected to large deformation by the extrusion of the bolt at point 2. At 1 m/s and 5 m/s loading speeds, the maximum strain value of point 2 increased with increasing loading speed but decreased significantly at 10 m/s loading speed. The maximum strain changes of point 2 were the same as the changes in deformation of aluminum alloy holes at different loading speeds, which were all related to the strain rate effect of aluminum alloy.

In order to understand the failure mechanism of the adhesive layer under different loading speeds, the peeling strain near the peak load of the adhesive layer was obtained. Figure 11(a) shows the strain state of the adhesive layer of the joint during the tensile process. It can be seen that in the early stage of the tensile process, the maximum peeling strain occurred at the end of the aluminum alloy. Cracks first appeared at the Al end. As the loading process proceeded, the peeling strain at the GFRP end also increased gradually and cracks began to appear at the GFRP end. Eventually, the cracks on both sides converged inside the adhesive layer and the layer lost its load-carrying capacity. Due to the larger stiffness of GFRP, the failure of the adhesive layer always started from the end of the aluminum alloy. The strain curve of the selected measuring points on the overlapping length

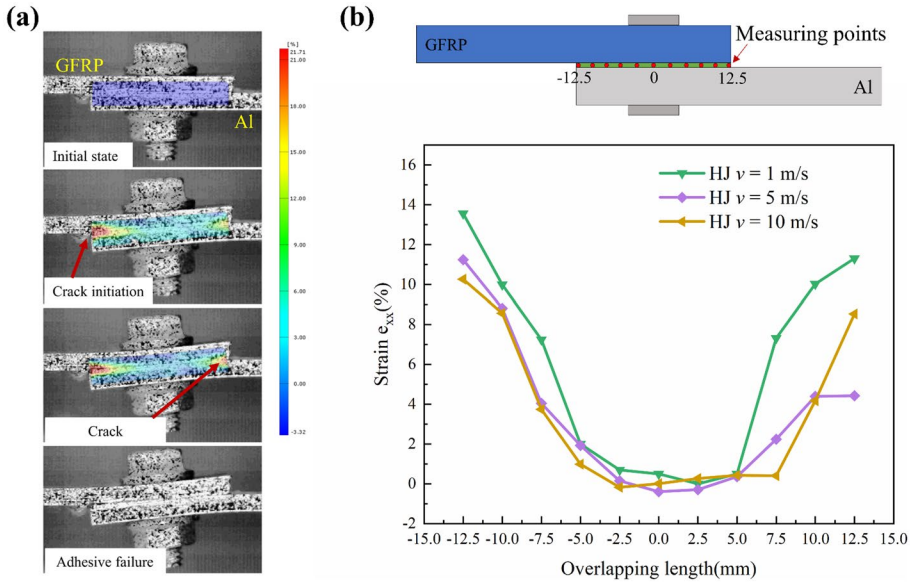


Fig. 11 Peeling strain analysis: **a** strain cloud map, **b** strain curve of the selected measuring points on the overlapping length

is shown in Fig. 11(b). The curves show that the loading rate has a significant effect on the peeling strain. It can be seen that the maximum peeling strain decreased with the increase of the loading speed, indicating that the plastic deformation of the adhesive layer decreased with the increase in loading speed. It also indicated that the adhesive layer showed an increasingly brittle nature when the loading speed was higher, which led to a change in the failure mode of the adhesive.

3.3 Fracture Analysis

For further failure analysis of specimens after the dynamic tensile test, the microscopic morphology of failure position at different loading speeds was analyzed. From the failure process, it can be seen that the GFRP in bolted joints experienced bearing failure first and eventually failed in cleavage under dynamic loading. Thus, the fracture surfaces for SEM were bearing failure region and cleavage failure region, as shown in Fig. 12(a). The bearing failure region and cleavage failure region were observed as shown in Fig. 12(b). In the bearing failure region, there were fiber bundle pull-outs and holes, with a large number of broken fibers and matrix fragments. The morphology in the cleavage failure region was mainly dominated by fiber bundle pullout. In order to further analyze the influence of loading speed on the failure of fiber and matrix, the morphology of the 90° fiber matrix under different loading speeds was analyzed. The morphology of 90° fiber in the bearing failure zone is shown in Fig. 12(c). It can be seen that the length of the pulled-out fibers gradually decreased as the loading speed increased, as did the number of matrix cracks and holes. The morphology of the 90° fiber matrix in the cleavage failure region is shown in Fig. 12(d). At a loading speed of 1 m/s, the fiber bundle collapsed into monofilament fibers that lost their integrity, and the monofilament fibers were uneven in length. With the increase in loading speed, the fracture surface of the

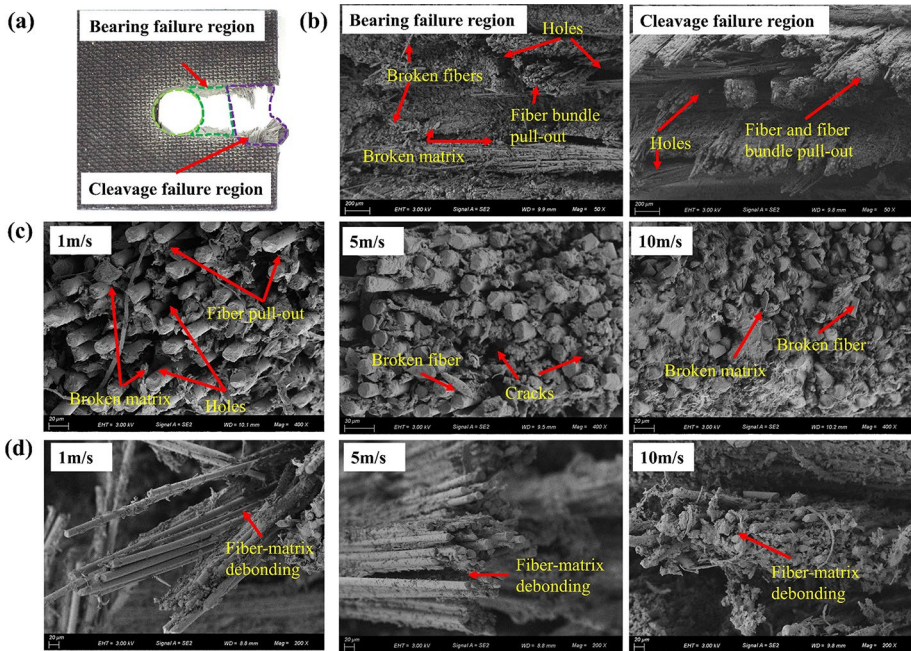


Fig. 12 a Sectioning for SEM observation; micromorphology of **b** the bearing failure zone and cleavage failure zone, **c** the 90° fibers in the shear failure zone, **d** the pull-out fiber bundles in the cleavage failure zone

fiber bundle became more and more flat, and the combination of fiber and matrix became more and more tight.

The difference in the microscopic morphology of the composite at different loading speeds can be attributed to the strain rate effect of the expansion of defects within the material. At lower loading speeds, due to the longer loading time, the defects inside the matrix were fully expanded and more cracks were formed. The binding force of the matrix on the fiber bundle was weakened, so there were more fibers pulled out. Meanwhile, the binding force of the matrix on the fiber bundle was also weakened. The fiber bundle collapsed into monofilament fibers and lost the overall bearing capacity. The monofilament fibers were damaged in their weak cross-section under the action of load, so the fiber fracture length was uneven. At higher loading rates, the defects in the matrix failed to expand sufficiently to form continuous cracks due to the short loading time [31–33]. The matrix maintained a strong binding force on the fibers and fiber bundles. The matrix and the fibers (or fiber bundles) were loaded as a whole under load until they together reached their ultimate strength when damage occurred. Therefore, the fracture surface was relatively flat, and the fiber and matrix still maintained a relatively strong interface bond after fracture.

4 Conclusions

In this paper, the mechanical properties and failure mechanisms of GFRP/Al bolted and hybrid joints under different loading speeds were investigated. The main conclusions were drawn as follows:

1. The peak load of bolted joints increased with the increase in loading speed. The peak load of hybrid joints under dynamic load was higher than that under static load, the incremental magnitude decreased by 8.64% when the loading speed was increased from 1 m/s to 10 m/s. The energy absorption of the hybrid joint was higher than that of the single bolted joint due to the fact that the adhesive layer absorbed part of the energy and increased the failure load of the joint.
2. For bolted joints, the failure modes of GFRP showed no significant correlation with loading speed, which were all shear-out failures. The loading speed had a significant effect on the microscopic morphology of the GFRP damage region. As the loading speed increased, the number of pulled-out fibers, holes, and cracks on the bearing failure region gradually decreased. The fracture surface also became flatter. The pulled-out fiber bundles were also more integral.
3. For the hybrid joint, the addition of the adhesive layer changed the failure mode of GFRP material from shear-out failures to tension failures due to the fact that the viscous action of the adhesive layer increased the yield strength of the hole. As the loading speed increased, the final failure area of GFRP in hybrid joints gradually decreased due to the strain rate effects on the expansion of internal defects in materials. Compared to static loading, the failure area of GFRP was reduced by 79.66% when the loading speed was increased from 1 m/s to 10 m/s. GFRP failed abruptly from a net-tension failure with almost no prior bearing damage at lower loading speeds (2 mm/min and 1 m/s). With the increase of loading speed, more amount of bearing damage preceded a final tension failure. The full-field strain analysis showed that the GFRP failed at smaller strains and became more brittle at higher loading speeds, which resulted in the GFRP failing first at the hole edge at higher loading speeds.
4. Deformation of the hole in aluminum alloy increased and then decreased with the increase in loading speed in both bolted and hybrid joints due to the strain rate effect on the aluminum alloy.

Acknowledgements This work was supported by National Key Research and Development Program of China (grant number: 2019YFE0124100) and National Natural Science Foundation of China (grant numbers: 52075380).

Author Contributions Hao Li: Conceptualization, Methodology, Investigation, Formal analysis, Writing — review & editing. Wei Du: Investigation, Analysis, Data curation, Writing — original draft. Xianming Meng, Sai Zhang, and Shipeng Li: Investigation, Funding acquisition. Yuxuan Cui and Wenchao Guo: Analysis, Data curation. All authors have read and agreed to the published version of the manuscript.

Declarations

Competing Interests The authors declare no competing interests.

References

1. Zhang, W., Xu, J. Advanced lightweight materials for Automobiles: A review. *Mater Des* 110994 (2022)
2. Wang, J., Shi, C., Yang, N., et al.: Strength, stiffness, and panel peeling strength of carbon fiber-reinforced composite sandwich structures with aluminum honeycomb cores for vehicle body. *Compos. Struct.* **184**, 1189–1196 (2018)
3. Machado, J.J.M., Gamarra, P.M.R., Marques, E.A.S., et al.: Numerical study of the behaviour of composite mixed adhesive joints under impact strength for the automotive industry. *Compos. Struct.* **185**, 373–380 (2018)
4. Ahmad, H., Markina, A.A., Porotnikov, M.V., et al.: A review of carbon fiber materials in automotive industry[C]/IOP Conference Series: Materials Science and Engineering. IOP Publishing **971**(3), 032011 (2020)
5. Mohammadi, H., Ahmad, Z., Mazlan, S.A., et al.: Lightweight Glass Fiber-Reinforced Polymer Composite for Automotive Bumper Applications: A Review. *Polymers* **15**(1), 193 (2022)
6. Sathishkumar, T., Satheshkumar, S., Naveen, J.: Glass fiber-reinforced polymer composites—A review. *J Reinf Plast Compos* **33**, 1258–1275 (2014)
7. Li, W., Shao, X., Li, L., et al.: Effect of hygrothermal ageing on the mechanical performance of CFRP/AL single-lap joints. *J. Adhes.* **98**(15), 2446–2473 (2022)
8. Liu, Y., Zhuang, W., Luo, Y., et al.: Joining mechanism and damage of self-piercing riveted joints in carbon fibre reinforced polymer composites and aluminium alloy. *Thin-Walled Struct.* **182**, 110233 (2023)
9. Zheng, G., He, Z., Wang, K., et al.: On failure mechanisms in CFRP/Al adhesive joints after hygrothermal aging degradation following by mechanical tests. *Thin-Walled Struct.* **158**, 107184 (2021)
10. Qin, X., Wang, C., Li, H., et al.: Experimental and numerical investigation on temperature field and joint tensile failure for CF/PPS-Al alloy interlocking induction welding. *Int. J. Adv. Manuf. Technol.* **127**(1), 795–813 (2023)
11. Chen, Y., Yang, X., Li, M., et al.: Mechanical behavior and Progressive failure analysis of riveted, bonded and hybrid joints with CFRP-aluminum dissimilar materials. *Thin-Walled Struct.* **139**, 271–280 (2019)
12. Paliwal, I., Ramji, M.: A detailed study on the damage evolution and failure assessment of single-lap hybrid joints in CFRP laminates under tensile loading. *Compos. Struct.* **299**, 116021 (2022)
13. Jiang, H., Sun, L., Liang, J., et al.: Shear failure behavior of CFRP/Al and steel/Al electromagnetic self-piercing riveted joints subject to high-speed loading. *Compos. Struct.* **230**, 111500 (2019)
14. Zuo, Y., Cao, Z., Cao, Y., et al.: Dynamic behavior of CFRP /Ti single-lap pinned joints under longitudinal electromagnetic dynamic loading. *Compos. Struct.* **184**(JAN), 362–371 (2017)
15. Egan, B., McCarthy, C.T., McCarthy, M.A., et al.: Static and high-rate loading of single and multi-bolt carbon-epoxy aircraft fuselage joints. *Compos. Part A: Appl Sci. Manufac.* **53**, 97–108 (2013)
16. Heimbs, S., Schmeer, S., Blaurock, J., et al.: Static and dynamic failure behaviour of bolted joints in carbon fibre composites. *Compos Part A: Appl Sci Manufac* **47**, 91–101 (2013)
17. Liu, X., Shao, X., Li, Q., et al.: Experimental study on residual properties of carbon fibre reinforced plastic (CFRP) and aluminum single-lap adhesive joints at different strain rates after transverse pre-impact. *Compos Part A: Appl Sci Manufac* **124**, 105372 (2019)
18. Wang, S., Liang, W., Duan, L., et al.: Effects of loading rates on mechanical property and failure behavior of single-lap adhesive joints with carbon fiber reinforced plastics and aluminum alloys. *Int J Adv Manuf Technol* **106**, 2569–2581 (2020)
19. Li, S., Sui, J., Ding, F., et al.: Optimization of milling aluminum alloy 6061-T6 using modified Johnson-Cook model. *Simul. Model Pract. Theory* **111**, 102330 (2021)
20. Li, Z., Xu, J., Demartino, C., et al.: Extremely-low cycle fatigue fracture of Q235 steel at different stress triaxialities. *J. Constr. Steel Res.* **169**, 106060 (2020)
21. Qin, G., Na, J., Mu, W., et al.: Effect of continuous high temperature exposure on the adhesive strength of epoxy adhesive, CFRP and adhesively bonded CFRP-aluminum alloy joints. *Compos. Part B: Eng.* **154**, 43–55 (2018)
22. Wei, S.: JingYu, Tong Weiping, Dynamic Mechanical Property of 6005A–T6 Aluminum Alloy for Automotive Use. *Rare Metal Mater. Eng.* **50**(06), 2118–2124 (2021)
23. Yang, X., Hector, L.G., Jr., Wang, J.: A combined theoretical/experimental approach for reducing ringing artifacts in low dynamic testing with servo-hydraulic load frames. *Exp Mech* **54**(5), 775–789 (2014)
24. Xiao, X.: Dynamic tensile testing of plastic materials. *Polym Test* **27**(2), 164–178 (2008)

25. Xu, P., Zhou, Z., Huang, W., et al.: The evolution mechanisms of bearing-tension-shear failure modes of FML joints under in-plane dynamic load. *Compos. Commun.* **32**, 101174 (2022)
26. Machado, J.J.M., Gamarra, P.M.R., Marques, E.A.S., et al.: Improvement in impact strength of composite joints for the automotive industry. *Compos. Part B: Eng.* **138**, 243–255 (2018)
27. Harris, J.A., Adams, R.D.: An assessment of the impact performance of bonded joints for use in high energy absorbing structures. *Proc. Inst. Mechan. Eng. Part C: J. Mechan. Eng. Sci.* 199(2):121–131 (1985)
28. Fu, Y., Yao, X.: A review on manufacturing defects and their detection of fiber reinforced resin matrix composites. *Compos. Part C: Open Access* **8**, 100276 (2022)
29. Huang, H., Talreja, R.: Effects of void Geometry on Elastic Properties of Unidirectional fiber Reinforced composites. *Compos. Sci. Technol.* 65(13), 1964–1981 (2005)
30. Mehdikhani, M., Gorbatikh, L., Verpoest, I., et al.: Voids in fiber-reinforced polymer composites: A review on their formation, characteristics, and effects on mechanical performance. *J. Compos. Mater.* **53**(12), 002199831877215 (2018)
31. Al-Zubaidy, H., Zhao, X.L., Al-Mahaidi, R.: Mechanical characterisation of the dynamic tensile properties of CFRP sheet and adhesive at medium strain rates. *Compos Struct* **96**, 153–164 (2013)
32. Naik, N.K., Yernamma, P., Thoram, N.M., et al.: High strain rate tensile behavior of woven fabric E-glass/epoxy composite. *Polym Test* **29**(1), 14–22 (2010)
33. Fei, G.U.O., Yanbin, L.I., Peiwei, Z.H.A.N.G., et al.: Quasi-static and dynamic shear properties of C/C composite pins. *Acta Materiae Compos. Sinica* **38**(5), 1604–1610 (2021)

Further Reading

34. Tucker, M.T., Horstemeyer, M.F., Whittington, W.R., et al.: The effect of varying strain rates and stress states on the plasticity, damage, and fracture of aluminum alloys. *Mech Mater* **42**(10), 895–907 (2010)
35. Acharya, S., Gupta, R.K., Ghosh, J., et al.: High strain rate dynamic compressive behaviour of Al6061-T6 alloys. *Mater Charact* **127**, 185–197 (2017)
36. Lee, W.S., Shyu, J.C., Chiou, S.T.: Effect of strain rate on impact response and dislocation substructure of 6061-T6 aluminum alloy. *Scripta Mater* **42**(1), 51–56 (1999)

Publisher's Note Springer Nature remains neutral with regard to jurisdictional claims in published maps and institutional affiliations.

Springer Nature or its licensor (e.g. a society or other partner) holds exclusive rights to this article under a publishing agreement with the author(s) or other rightsholder(s); author self-archiving of the accepted manuscript version of this article is solely governed by the terms of such publishing agreement and applicable law.